RSC Advances

PAPER

View Article Online
View Journal | View Issue

Cite this: *RSC Adv.*, 2026, **16**, 18724

Physicochemical modulation of liquid crystal anchoring energy *via* nanopatterned BiTiO/polymer hybrid interfaces

Dong Hyun Kim,*[b] Yoon-Seok Choi,*[b] Han-Jin Seo,*[b] Seoung-Soo Shin,*[b] Jong-Yeon Woo,*[b] Seung-Jin Park*[b] and Dae-Shik Seo *[a]

High-performance liquid crystal (LC) alignment layers are essential for optimizing the electro-optic properties of advanced display and photonic devices. While conventional rubbing processes are widely used, they face limitations such as physical contact damage and static electricity. In this study, we present a robust non-contact alignment method by transferring one-dimensional nanopatterns onto an ultraviolet-responsive polymer and a BiTiO hybrid film using ultraviolet nanoimprint lithography (UV-NIL). The effects of UV curing time (2, 4, and 6 min) on the morphological stability and surface modification of the films were systematically analyzed to verify their performance as LC alignment layers. Our results demonstrate that LC cells fabricated with BiTiO hybrid thin films cured for 4 min achieved superior homogeneous alignment, as confirmed by polarized optical microscopy (POM) and pretilt angle measurements. Atomic force microscopy (AFM) revealed that the optimal curing time is critical for the formation of well-defined nanopatterns. Furthermore, the developed films exhibited a high average anchoring energy of 1.9×10^{-4}, which is comparable to conventional alignment methods. These findings highlight the potential of nanopatterned hybrid thin films as a highly efficient and stable alternative for next-generation LC alignment applications.

Received 5th January 2026
Accepted 10th March 2026

DOI: 10.1039/d6ra00107f

rsc.li/rsc-advances

1 Introduction

The refractive index and dielectric anisotropy of liquid crystals (LCs) have shown effective performances for their use in implementing modern displays. LCs are the most widely used materials in the display industry, from small displays such as mobile device screens to large displays such as television panels. Additionally, as the scope of the users' electronic device demands expands, the LC display (LCD) market has grown. In the current technology used to produce LCDs, a layer called the LC alignment layer is required to control the LC molecules as desired. Recent studies have focused on enhancing the performance of liquid crystal (LC) devices through precise alignment control and reduction of operating voltages. For instance, surface acoustic waves (SAWs) have been employed to induce mechanical vibrations in LC lattices, successfully achieving a highly uniform monodomain structure with minimized defects. Furthermore, the integration of high-aspect-ratio nanowall electrodes has demonstrated significant improvements in electro-optic properties, notably reducing the operating voltage by generating strong transverse electric fields within a small sub-electrode gap. These advancements highlight the critical role of nanostructured surfaces and external physical stimuli in optimizing the alignment order and electrical efficiency of LC systems.[1,2]

The LC alignment film is a very important component because it allows the LC molecules to be aligned vertically or horizontally and can be switched using an electric field.[3–8] A representative technology for creating such LC alignment films is the rubbing method used to obtain polyimide (PI) films. This method involves creating physical grooves in a polymer thin film using a rotating cloth and has been used as a representative orientation method for a long time. However, since this method is based on contact and friction, static electricity and scratches may occur on the films, in addition to issues such as microdefects.[9–12] To address these shortcomings, oblique deposition, ion-beam irradiation, photoalignment, and brush-coating methods have been developed and used. In the present study, instead of the rubbing method, we transfer a one-dimensional nanopattern through nanoimprint lithography (NIL) and introduce a method wherein this pattern induces orientation by restricting the physical movements of the LC molecules. NIL is suitable for large-area processing because its pattern-replication-based molding process ensures cost-effectiveness and high throughput. Unlike other lithography processes that require pattern masks and photoresist along

[a]*IT Nano Electronic Device Laboratory, Department of Electrical and Electronic Engineering, Yonsei University, 50 Yonsei-ro, Seodaemun-gu, Seoul 120-749, Republic of Korea. E-mail: dsseo@yonsei.ac.kr*

[b]*Department of Electronic Engineering, Cheongju University, 298 Daesung-ro, Cheongju 28503, Republic of Korea*

with being difficult to utilize, NIL has the advantage of being able to transfer nanoscale patterns in a relatively effective manner. This method is therefore mainly used in semiconductors, solar energy production, *etc.*, but has been adopted to produce LCD alignment films because it can be used very effectively. NIL is classified into thermal and ultraviolet NIL types depending on the method of curing the target thin films after transferring the patterns.[13–17] UV-NIL uses UV-reactive polymers for curing. Since thermal NIL requires high heat and pressure, there is risk of damage to the thin film; hence, in this study, alignment films were produced by mixing a UV-reactive polymer with a solution of bismuth titanium oxide. Through the solution process, a one-dimensional pattern was transferred to a hybrid BiTiO solution film and UV-reactive polymer to homogeneously align the LC molecules.[18,19] Atomic force microscopy (AFM) was used to analyze and confirm the clarity and uniformity of the patterns, and X-ray photoelectron spectroscopy (XPS) was used to confirm whether the bismuth and titanium molecules were deposited well on the pattern. The transmittances of the produced thin films were analyzed using UV-Vis-NIR spectroscopy. To confirm the LC alignment performance, polarized optical microscopy (POM) and pretilt angle measurements were used, and the electro-optical performance was assessed through anchoring energy measurements.

2 Experimental methods

2.1 Polymer/inorganic hybrid solution preparation

The BiTiO solution was prepared by adding 0.1 M bismuth nitrate pentahydrate (≥99.99% trace metals basis, Sigma-Aldrich) and 0.1 M titanium dioxide (nanotubes, 25 nm average diameter, Sigma-Aldrich) to 2-methoxyethanol (ReagentPlus®, ≥99.0%, contains 50 ppm BHT as stabilizer, Sigma-Aldrich) and stirring at 360 rpm and 70 °C for 4 h. Thereafter, it was aged for 1 day to achieve a stable state. The UV-responsive polymer consisted of three acrylic monomers: dipentaritol hexaacrylate, tripropylene glycol di-acrylate, and 2-hydroxyethyl acrylate. A hybrid solution was prepared by mixing 10 wt% of the UV-reactive polymer in a bismuth titanium oxide solution with stirring at 420 rpm for 1 h.

2.2 Polydimethylsiloxane (PDMS) mold fabrication for nanoimprint

A rigid-flex mold is typically required for the UV-NIL process. The mold must be rigid enough to sufficiently transfer the pattern and allow UV rays to be projected through the curing process while also being sufficiently flexible to enable roll-to-roll processing. We prepared a PDMS mold as the most suitable material for this purpose. It is easy to engrave nanopatterns on PDMS by adding a patterned Si wafer during the curing process. Patterned Si wafers used for this purpose were prepared using UV interference through a Lloyd mirror. The one-dimensional nanopatterns were then transferred using the interference phenomenon between the laser energy that is directly incident on the wafer and energy that is reflected by a mirror before incidence. The Si wafer produced in this manner was fixed in a mold for PDMS production; liquid PDMS (Sylgard-184, Dow Corning) was poured over it, and the air bubbles were removed in vacuum for 2 h. After curing the PDMS mold, it was cut into samples of size 32 mm × 22 mm × 1.1 mm to prepare the LC cells. Indium tin oxide (ITO) glass (32 mm × 22 mm × 1.1 mm, sheet resistance: 10 Ω sq^{-1}, Samsung Corning 1737) used as the thin-film substrate was sonically washed in acetone and isopropyl alcohol for 10 min each, wiped with deionized water, and cleaned with N_2 gas.

2.3 Pattern transfer from the PDMS mold to hybrid film

The hybrid solution was dropped on the prepared ITO glass and spin coated at 3000 rpm for 30 s to prepare a film of uniform thickness. When the PDMS mold is attached to a uniformly produced liquid film, the hybrid solution enters the spaces between the patterns by capillary force. The pattern of the PDMS mold was thus transferred to the spin-coated solution in the form of an engraving, which was then exposed in this state to a UV light emitter. A 1 kW mercury lamp was used for the UV exposure, with its energy density set to 7.9 mW cm^{-2}. The hybrid film samples were cured for 2, 4, and 6 min by exposure to UV rays. When the PDMS mold was separated after UV exposure, a hybrid film with the transferred mold pattern was produced. The acrylic monomers in the UV-curable polymer exist in the liquid state in the hybrid solution but crosslinking occurs when exposed to UV so that the curing reaction begins.

2.4 Surface analyses and LC alignment observations

To confirm the nanopatterns transferred to the surfaces of the BiTiO hybrid films, they were observed using AFM (XE-200, Park Systems). The chemical composition and deposition of the BiTiO hybrid films were analyzed using XPS (K-alpha, Thermo VG, UK). POM (BXP51, Olympus) and pretilt angle measurements (TBA 107, Autronic) were also performed to analyze the LC alignment. The liquid crystal (LC) material used in this study is IAN-5000XX T14(IAN-5000XX T14, JNC Co., $n_e = 1.595$, $n_o = 1.484$, $\Delta n = 0.111$, $\Delta\varepsilon = 10.3$, $T_c = 81.8$ °C). The capacitance–voltage (C–V) characteristics of the LC cells were measured using an LCR meter.

3 Results and discussion

The purpose of this study is to determine the most effective UV curing time for a hybrid solution prepared by adding a UV-curable polymer to a solution of BiTiO. In this study, UV curing was performed for 2, 4, and 6 min, and the resulting hybrid thin films were analyzed. Additionally, the hybrid thin films were assembled into antiparallel LC cells to evaluate the LC alignment performances.

Fig. 1 shows the AFM images of the nanopatterned BiTiO hybrid films that were cured under UV for 2, 4, and 6 min. In the film cured for 2 min (Fig. 1(a)), the engraved pattern of the PDMS mold is visible. According to Berreman's groove orientation theory, LC molecules in periodic grooves receive a force that minimizes the free energy, and this force is proportional to the height of the groove.[20–23] Although the groove height may be

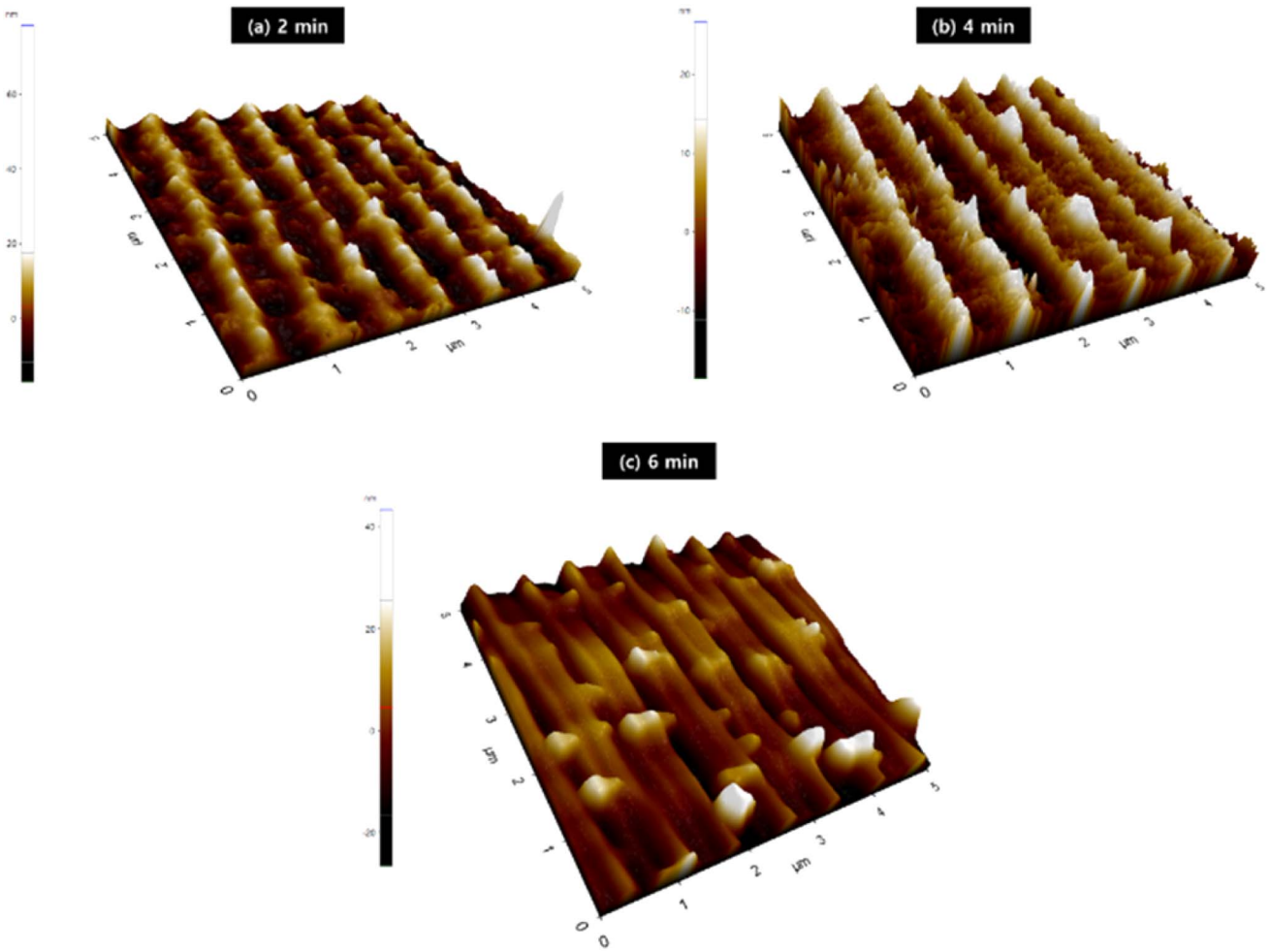

Fig. 1 Surface AFM images of BiTiO thin films patterned *via* NIL UV-cured for (a) 2 min, (b) 4 min, and (c) 6 min.

affected by the pattern's period or other parameters, since such factors are not affected by the UV curing time, this study focused on the height of the pattern. In the film cured for 4 min, a clear pattern was formed, as shown in Fig. 1(a), and a larger pattern height could be confirmed. This increase in pattern height is likely to increase the force with which the LC molecules try to align, leading to more stable alignment effects. However, when the UV irradiation time was further extended to 6 min, it was confirmed that the grooves of the mold became significantly thicker. This is expected to have negative effects on the alignment mechanism by lowering the periodicity of the grooves and reducing the volume of the grooves where LC molecules can exist.

Fig. 2 shows the optical transmittance analyzed by UV-Vis-NIR spectroscopy. The transmittances in the visible range of 400–800 nm for the nanopatterned BiTiO hybrid films cured for 2, 4, and 6 min were 87.6, 85.6, and 81.2%, respectively. Considering that the alignment films must have transmittances over 80% to be used in display devices, the obtained results pose no problems. However, unlike the 4 min cured sample, which showed a high transmittance of over 85%, a significant decrease in transmittance was observed for the 6 min cured sample. Since there was no difference in the material, this difference may be considered an effect of the change in the surface structure, as confirmed by AFM.

Fig. 3 shows the XPS spectra of the UV-cured BiTiO hybrid films. Each XPS spectrum was analyzed through peak deconvolution, and the peaks of Bi 4f and Ti 2p were identified to confirm whether Bi and Ti elements were well deposited on each of the films. The Bi 4f component appeared as two peaks, namely Bi $4f_{7/2}$ and Bi $4f_{5/2}$, owing to spin–orbit separation. The Bi $4f_{7/2}$ peak had binding energies of 158.3, 158.2, and 158.3 eV for the samples cured for 2, 4, and 6 min, respectively, and the peak shift was not significant. The Bi $4f_{5/2}$ peak also showed no peak shifts from its binding energies of 163.6, 163.5, and 163.6 eV. However, a higher peak intensity was observed for the 4 min cured sample compared to the 2 min sample, and the height decreased again for the 6 min sample. The Ti 2p component also appeared as two peaks, namely Ti $2p_{3/2}$ and Ti $2p_{1/2}$, owing to spin–orbit separation. The Ti $2p_{3/2}$ peak had binding energies of 457.6, 457.5, and 457.6 eV for the samples cured for 2, 4, and 6 min, respectively, with no significant changes in the peaks. Similarly, the Ti $2p_{1/2}$ peaks were observed at 464.2, 464.3, and 464.6 eV. However, in Ti 2p, as in Bi 4f,

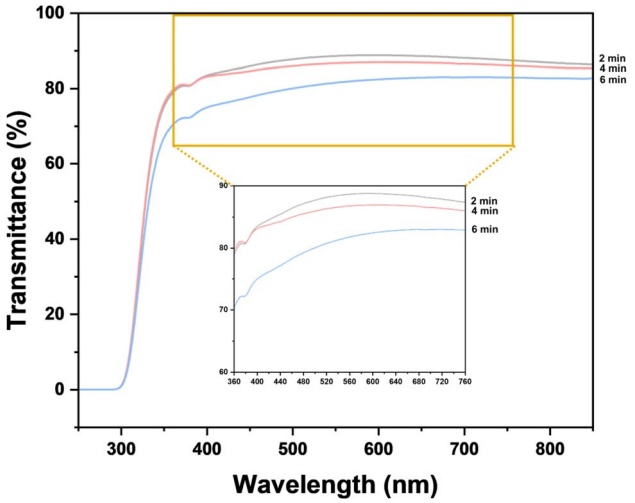

Fig. 2 UV-Vis-NIR transmittance plots of BiTiO thin films patterned *via* NIL UV-cured for 2, 4, and 6 min. Measurements were made at wave lengths from 250 nm to 850 nm, and the graph was expanded from 350 nm to 750 nm, which is the visible range.

a higher peak was noted for the 4 min cured sample compared to the 2 min sample, and it was found to be lower again for the 6 min sample. The increase and decrease in these peaks is believed to be due to the cross-linking phenomenon of the hybrid film caused by UV curing, which peaked at 4 min; however, the bonds broke down when more UV was applied.

Based on the surface analyses, antiparallel LC cells were fabricated using the BiTiO hybrid films on which nanopatterns were transferred and LC alignment characteristics were analyzed (Fig. 4). The dark optical textures observed in Fig. 4 are attributed to the homogeneous alignment of the LC molecules in an anti-parallel cell configuration. Under crossed-polarized optical microscopy, an extinction state appears when the director of the homogeneously aligned LCs is oriented parallel to the transmission axis of either the polarizer or the analyzer. This result demonstrates that a high-quality, uniform planar alignment was successfully induced across the entire patterned area. Samples cured for 2 min showed some reverse-tilt disclinations. When the LC molecules are oriented in opposite directions, light leakage occurs between the LC molecules and line defects are discovered in POM, which is called the reverse-tilt disclination phenomenon. In other words, this phenomenon is an indicator of the points where the LC molecules are not aligned homogeneously, which means that there were some areas where alignment failed in the 2 min sample. In contrast, the 4 min sample showed perfect alignment. If all LC molecules are aligned in one direction in POM, all light is blocked by the analyzer and polarizer that are placed orthogonal to each other, and a dark image is observed. When the analyzer and polarizer are parallel, all light passes through, and a white image is observed. Therefore, a 4 min sample showing completely dark and completely white images is an indicator that good homogeneous alignment has been achieved. However, in the 6 min sample, reverse-tilt disclinations occurred as in the 2 min sample, indicating that the alignment was not perfect.

Fig. 5 shows the pretilt angle measurements. These curves measured using the crystal rotation method are obtained by transmitting a HeNe laser through an LC cell rotated from −70° to 70°. The blue and red lines in the graph represent simulation and experimental results, respectively. The higher the match between these two lines, the more stable is the alignment of the LC molecules. Similar to the results of POM, the highest similarity can be seen in the 4 min sample.

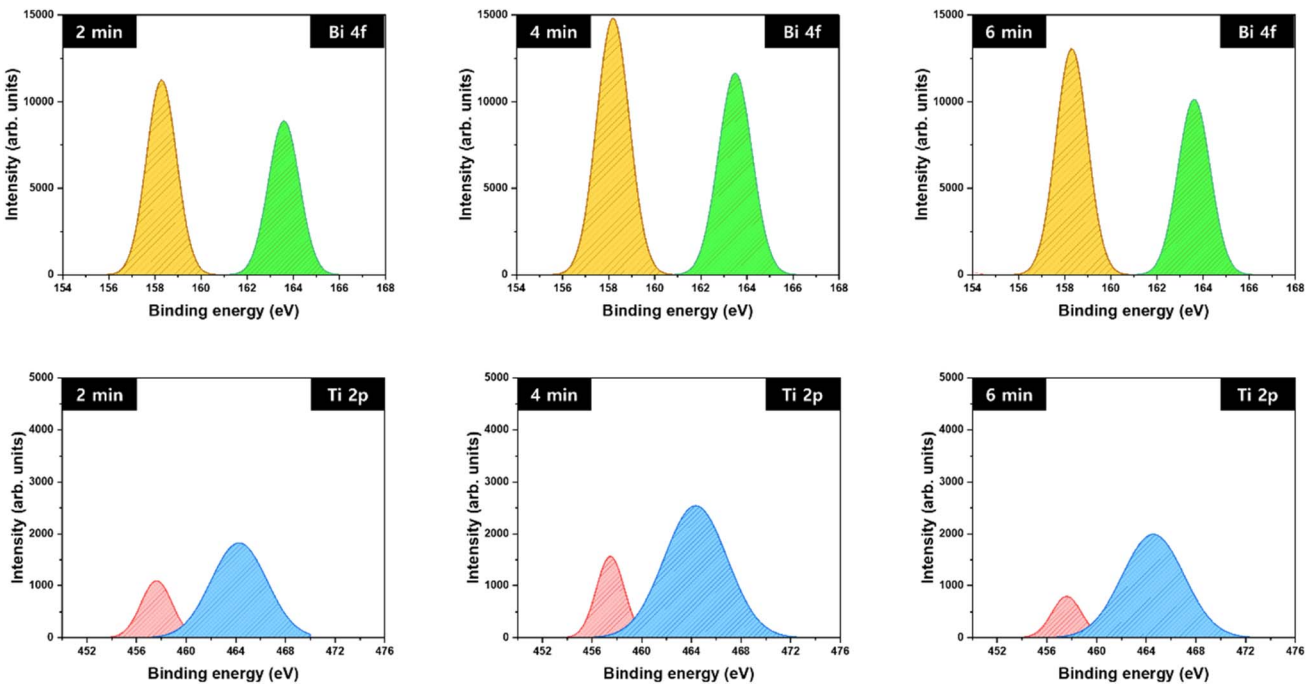

Fig. 3 XPS images of BiTiO thin films patterned *via* NIL UV cured for 2, 4, and 6 min. Deconvoluted peaks for Bi 4f and Ti 2p are shown.

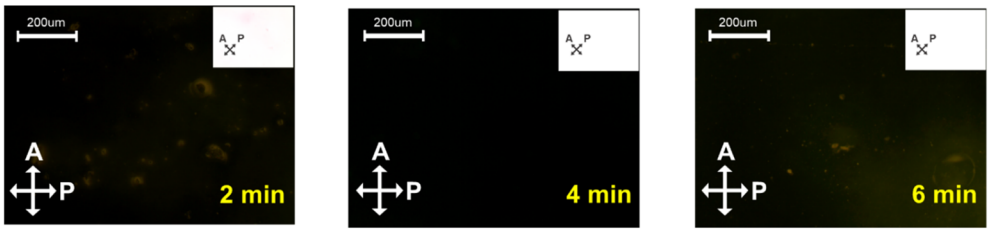

Fig. 4 POM image of antiparallel cells fabricated from BiTiO thin films patterned through NIL UV cured for 2, 4, and 6 minutes. Black images indicate that the analyzer and polarizer are orthogonal, and white images indicate that both polarizers are rotated by 45°.

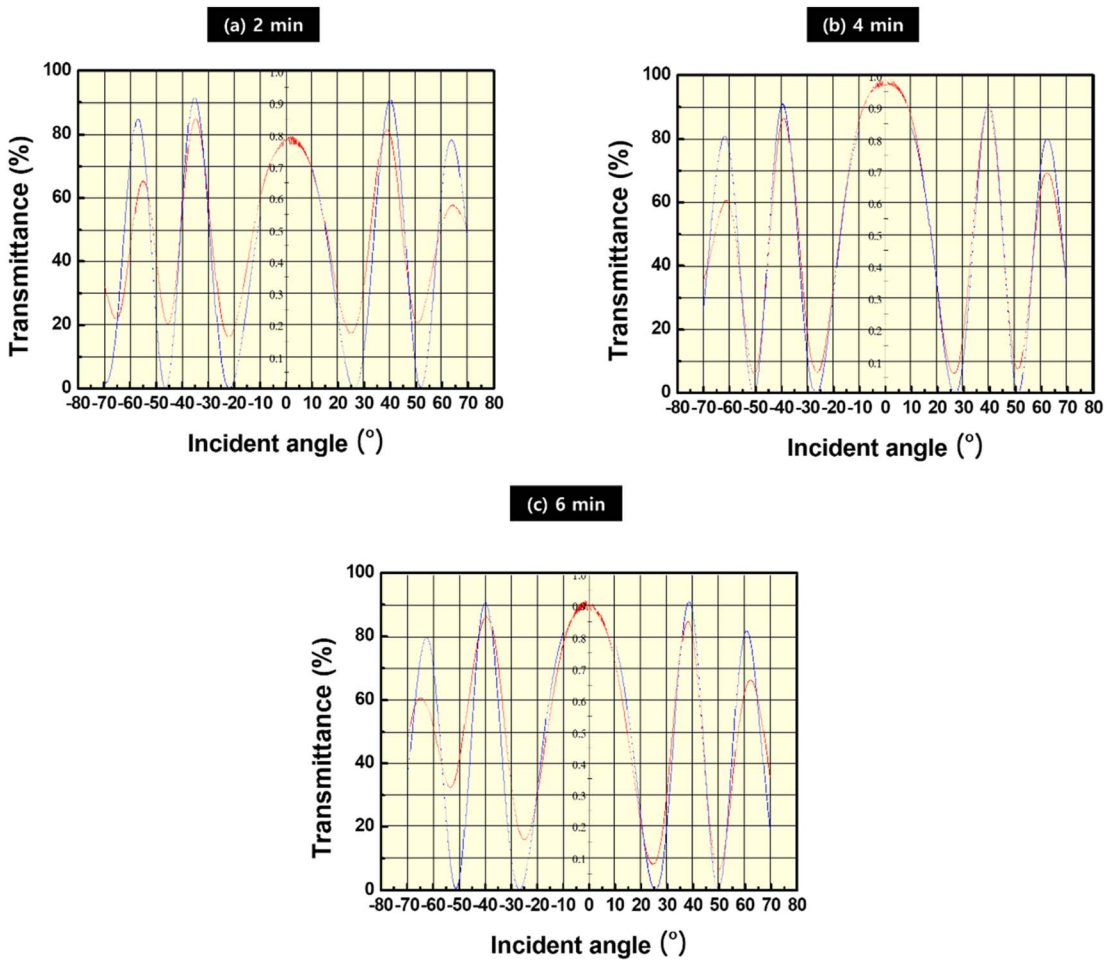

Fig. 5 Tilt-bias-angle graph of antiparallel cells fabricated from BiTiO thin films patterned through NIL UV cured for (a) 2 min, (b) 4 min, and (c) 6 min.

In Fig. 6, the results of the anchoring energy measurements are confirmed *via* voltage–relative capacitance graphs. The anchoring energy refers to the force that holds the LC molecules on the surface of the film. The anchoring energy was determined from the measured C–V data using the Yokoyama-van Sprang high-field method. By analyzing the linear relationship between the capacitance and the reciprocal of the applied voltage ($1/V$) in the high-voltage regime, we extracted the effective extrapolation length (d_e). The anchoring energy (W) was then calculated based on the relation between d_e and the elastic constant of the LC, providing a quantitative measure of the surface alignment strength. The stronger this force, the more stable is the alignment of the molecules. The anchoring energies for the samples cured for 2, 4, and 6 min were found to be 6.8×10^{-5}, 1.9×10^{-4}, and 9.0×10^{-5}, respectively. As with the previous orientation characteristic graphs, the highest anchoring energy was confirmed at 4 min. Anchoring energy refers to the interaction strength between liquid crystal molecules and the alignment surface. While conventional rubbing processes are known for providing strong alignment, our results

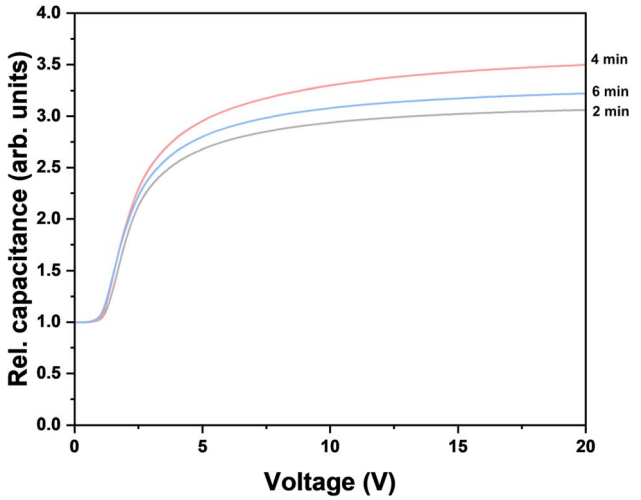

Fig. 6 *C–V* curves of cells fabricated from BiTiO thin films patterned *via* NIL UV cured for 2, 4, and 6 min. Measured to determine the anchoring energy of the liquid crystal cell.

demonstrate that the nanopatterned surfaces can achieve a comparable level of anchoring energy. This indicates that nanopatterning is a viable and effective alternative for achieving stable LC alignment without the mechanical contact or static electricity issues associated with rubbing.

In conclusion, when UV curing was carried out for 2 min, the nanopattern was not sufficiently transferred, so sufficient results could not be obtained in terms of the LC alignment and electro-optical characteristics. When UV curing was performed for 4 min, the nanopattern appeared clearly, and the height of the groove increased, allowing the LC molecules to align strongly. This also allowed improvements in the LC alignment characteristics and electro-optical properties. However, when UV curing was conducted for 6 min, the shape of the pattern was damaged, which led to a deterioration of the LC alignment and electro-optical properties. Additionally, there was a serious loss in transmittance, reducing the value of the film for use in display devices. Hybrid LC alignment films using UV-NIL can achieve stable LC alignment characteristics using this easy method and have high potential for next-generation alignment film production.

4 Conclusions

One-dimensional nanopatterns were successfully transferred to a UV-responsive polymer and BiTiO hybrid thin films using the UV-NIL method. These nanopatterns limit the free energy of the LC molecules according to the Berreman model, inducing uniform alignment in a specific direction. By integrating the structural stability of inorganic BiTiO with the high processability of UV-responsive polymers, this work addresses the research gap of maintaining high alignment stability in non-contact methods. In this work, the UV curing time was controlled to 2, 4, and 6 min; further, the nanopatterns and surface modifications were analyzed to verify their performances as LC alignment films. Through AFM analysis, it was confirmed that the patterns became well-defined, with the groove height increasing as the curing time increased from 2 to 4 min. However, at 6 min of curing, the pattern became blurred, and the effective volume for LC molecule arrangement decreased, which negatively affected transmittance, orientation, and electro-optical properties.When the LC cell made of the hybrid thin film was cured for the optimal 4 min, a perfectly homogeneous POM image was obtained, validated by pretilt angle measurements. Notably, despite being a non-contact method, our approach successfully achieved a high anchoring energy of 1.9×10^{-4}, nearing the high standards typically exclusive to conventional rubbing. This highlights the enhanced reliability of our hybrid nanopatterning as a robust alternative. These results confirm the potential of the developed hybrid thin film as an excellent LC alignment layer for next-generation display applications.

Conflicts of interest

There are no conflicts to declare.

Data availability

The data supporting this article have been included as part of the supplementary information (SI). Supplementary information is available. See DOI: https://doi.org/10.1039/d6ra00107f.

Acknowledgements

This research was supported by the Regional Innovation System & Education (RISE) program through the Chungbuk RISE, funded by the Ministry of Education (MOT) and the Chungcheongbuk-do, Republic of Korea. (2025-RISE-11-013-03)

References

1 T.-H. Chiang, *et al.*, Electro-optic properties of liquid crystal cells with nanowall electrodes, *Opt. Lett.*, 2023, **48**(21), 5623–5626, DOI: 10.1364/OL.505221.
2 H. Suryantari, *et al.*, Formation of monodomain polymer-stabilized blue phase liquid crystals using surface acoustic waves, *Opt. Lett.*, 2022, **47**(24), 6333–6336, DOI: 10.1364/OL.475938.
3 M. L. Brongersma, Y. Cui and S. Fan, *Nat. Mater.*, 2014, **13**, 451.
4 J. Sang, L. Han, M. Liu, J. Shang, J. Sun, L. Guo, D. Ge, Y. Zhang, S. Zhao and V. G. Chigrinov, *ACS Appl. Nano Mater.*, 2021, **4**, 12937, DOI: 10.1021/acsanm.1c03140.
5 H. Lee, *J. Vac. Sci. Technol. B Microelectron. Nanomater. Struct.*, 2005, **23**(3), 1102.
6 H. Y. Kim, Y. J. Park, J. Kim, *et al.*, *Adv. Funct. Mater.*, 2016, **26**, 3454.
7 P. Chaudhari, J. Lacey, J. Doyle, E. Galligan, S. C. A. Lien, A. Callegari, G. Hougham, N. D. Lang, P. S. Andry, R. John, K. H. Yang, M. Lu, C. Cai, J. Speidell, S. Purushothaman, J. Ritsko, M. Samant, J. Stöhr, Y. Nakagawa, Y. Katoh,

Y. Saitoh, K. Sakai, H. Satoh, S. Odahara, H. Nakano, J. Nakagaki and Y. Shiota, *Nature*, 2001, **411**(6833), 56.
8 C. V. Ramana, E. J. Rubio, C. D. Barraza, A. M. Gallardo, S. McPeak, S. Kotru and J. T. Grant, *J. Appl. Phys.*, 2014, **115**(4), 043508.
9 J. C. Armas-Pérez, X. Li, J. A. Martínez-González, *et al.*, *Langmuir*, 2017, **33**, 12516.
10 H.-C. Jeong, J. H. Lee, J. Won, B. Y. Oh, D. H. Kim, D. W. Lee, I. H. Song, Y. Liu and D.-S. Seo, *Opt. Express*, 2019, **27**(13), 18094.
11 S. W. Ahn, K. D. Lee, J. S. Kim, S. H. Kim, J. D. Park, S. H. Lee and P. W. Yoon, *Nanotechnology*, 2005, **16**, 1874, DOI: 10.1088/0957-4484/16/9/076.
12 T. Ube, H. Tsunoda, K. Kawasaki and T. Ikeda, *Adv. Opt. Mater.*, 2021, **9**, 1.
13 W. K. Lee, Y. S. Choi, Y. G. Kang, *et al.*, *Adv. Funct. Mater.*, 2011, **21**, 3843.
14 Y. Hirai, S. Yoshida and N. Takagi, *J. Vac. Sci. Technol. B Microelectron. Nanomater. Struct.*, 2003, **21**(6), 2765.
15 C. T. Mattew, L. Whitney and N. T. Van, *Annu. Rev. Chem. Biomol. Eng.*, 2016, **7**, 583.
16 S. Edinger, N. Bansal, M. Bauch, R. A. Wibowo, G. Újvári, R. Hamid, G. Trimmel and T. Dimopoulos, *J. Mater. Sci.*, 2017, **52**, 8591, DOI: 10.1007/s10853-017-1084-8.
17 M. Lu, *Jpn. J. Appl. Phys.*, 2004, **43**(12), 8156.
18 I. H. Song, H. C. Jeong, J. H. Lee, *et al.*, *Adv. Opt. Mater.*, 2021, **9**, 1.
19 S. Yang, D. H. Cho, M. K. Ryu, S. H. K. Park, C. S. Hwang, J. Jang and J. K. Jeong, *Appl. Phys. Lett.*, 2010, **96**, 213511, DOI: 10.1063/1.3432445.
20 D. W. Berreman, *Phys. Rev. Lett.*, 1972, **28**, 1683.
21 J. I. Fukuda, M. Yoneya and H. Yokoyama, *Phys. Rev. Lett.*, 2007, **98**, 1.
22 H. Yokoyama, *J. Appl. Phys.*, 1985, **57**, 4520.
23 H. Yokoyama, S. Kobayashi and H. Kamei, *J. Appl. Phys.*, 1987, **61**, 4501.